Available online at www.sciencedirect.com
ScienceDirect
Journal of the European Ceramic Society 29 (2009) 717–723
www.elsevier.com/locate/jeurceramsoc

Effect of repeated composite sol infiltrations on the dielectric and piezoelectric properties of a $Bi_{0.5}(Na_{0.82}K_{0.18})_{0.5}TiO_3$ lead free thick film

Haibo Zhang *, Shenglin Jiang

Engineering Research Centre for Functional Ceramics MOE, Department of Electronic Science and Technology, Huazhong University of Science and Technology, Wuhan 430074, PR China

Received 27 March 2008; received in revised form 20 July 2008; accepted 22 July 2008
Available online 6 September 2008

Abstract

$Bi_{0.5}(Na_{0.82}K_{0.18})_{0.5}TiO_3$ lead free thick films have been produced using a combination of screen printing and subsequent infiltration of corresponding composite sol. Their structure, dielectric, ferroelectric and piezoelectric properties were investigated with variation in the number of composite sol infiltrations and the nanopowder loading in composite sol. Dielectric constant, remanent polarization, and piezoelectric coefficient have been shown to increase with increasing numbers of composite sol infiltration. Dielectric and ferroelectric properties of the thick films are found to be strongly dependent on the powder concentration of composite sols. The resulting 40 μm thick films infiltrated with 1.5 g/ml composite sols have maximum relative permittivity of 569 (at 10 kHz), remanent polarization of 21.3 μC/cm^2, coercive field of 80 kV/cm, and longitudinal effective piezoelectric coefficient $d_{33\text{eff}}$ of 109 pm/V. The performance of these lead free piezoelectric thick films is comparable to the corresponding bulk ceramics.

Keywords: Screen printing; Thick films; Lead free piezoelectric; Potassium sodium bismuth titanate

1. Introduction

Piezoelectric thick films are of major interest in the actuation of active structures in MEMS, they have been widely applied to micropumps,[1,2] ultrasonic motors,[3] resonators,[4] microfluidic separators,[5] high-frequency transducers,[6] and energy harvesting,[7] because they exhibit properties such as larger displacement and quick response, high frequency, and can be precisely controlled. The thick films are difficult to produce using lapping and machining bulk ceramics due to the expense, waste and difficulty in handling the ceramics, on the other hand, most of the thin film processing, such as sol–gel, sputtering, physical vapour deposition, chemical vapour deposition, and pulsed laser deposition are not practical due to the slow deposition rates and high levels of stress generated during processing which can lead to cracking of the film. The thick films technologies filled the gap between bulk materials and thin films. Many studies have been reported on the preparation of piezoelectric thick films by screen printing, tape casting, composite sol–gel, electrophoretic deposition, ink-jet printing, and aerosol deposition. Screen-printing technology has an advantage in that it enables low-cost fabrication of a device and device array in desired pattern without a photolithography.

So far, we found almost all piezoelectric thick films are lead-based materials, the toxicity of lead oxide has been considered to be a serious threat to the environment. Therefore, research on lead free replacement has become more and more concentrated in the last few years.[8] But the studies on lead free materials are almost limited in bulk ceramics, only several attempts at the fabrication of lead free thin film have been made.[9] There is a lack of reports on the fabrication of the lead free piezoelectric thick films. Bismuth sodium titanate, $(Bi_{0.5}Na_{0.5})TiO_3$ (NBT), is considered to be an excellent candidate as a key material of lead free piezoelectric material because NBT is strongly ferroelectric with relatively large remanent polarization, $P_r = 38\ \mu C/cm^2$, the strong ferroelectricity of NBT-based solid solution is attributed to $(Bi_{0.5}Na_{0.5})^{2+}$ ions, especially Bi^{3+} ions, of A-site on perovskite structure(ABO_3).[10,11] It has been reported that NBT ceramics modified with $BaTiO_3$ (BT)[12] or $Bi_{0.5}K_{0.5}TiO_3$ (KBT)[13] showed improved dielectric

* Corresponding author. Tel.: +86 27 87542693; fax: +86 27 87542693.
E-mail address: changhb@gmail.com (H. Zhang).

0955-2219/$ – see front matter © 2008 Elsevier Ltd. All rights reserved.
doi:10.1016/j.jeurceramsoc.2008.07.049

and piezoelectric properties because there existed the corresponding rhombohedral tetragonal MPB. Sasaki et al. reported their work on NBT–KBT system and showed that maximum electromechanical coupling factor and dielectric constant were obtained around the MPB region.[14]

It is still a challenge to make piezoelectric thick films by screen printing, this is due to low density result in constrained sintering and the residual organic vehicle in green films. Several attempts such as isostatic pressing, addition of sintering aids,[15] and sol infiltration to increase the density of the thick film[16] have been made. However, the presence of significant levels of non-function material within the thick film can reduce the electric properties by addition of sintering aids, and the density cannot be effectively increased by sol infiltration due to the limited solid content in the precursor solution. In this study, the composite sols containing precursor solution and nanopowders with same composition were used to replace the simple sols in thick film infiltration treatment. The $Bi_{0.5}(Na_{1-x}K_x)_{0.5}TiO_3$ (abbreviated to NKBT) nanopowders were prepared by sol–gel technique. NKBT thick films were prepared on alumina substrate using a screen-printing method, in which the NKBT composite sol was spin coated on the thick films. Their structure and electrical properties were investigated with variation in the number of composite sol coatings and the nanopowder loading in composite sol.

2. Experimental

2.1. Composite sols production

Sodium acetate($(CH_3COO)Na{\cdot}3H_2O$), potassium acetate (CH_3COOK), bismuth nitrate ($Bi(NO_3)_3{\cdot}5H_2O$), tetrabutyl titanate ($Ti(OC_4H_9)_4$) were used as starting materials, sodium acetate, potassium acetate, and bismuth nitrate were dissolved in glacial acetic acid (CH_3COOH) and triethanolamine was added as a catalyst. Tetrabutyl titanate was dissolved in glycol ether and acetylacetone was used to stabilize the solution, all above reagents were at analytic purity. NKBT precursor solutions were prepared by mixed the above two solutions, and the concentration of solution was controlled to 0.4–0.6 mol/L by diluting with methoxy ethanol. The resultant solution was stirred at room temperature for more than 24 h to yield a clear, stable and homogeneous sol. NKBT nanopowders were prepared from the sols the PH of the sol was adjusted with nitric acid to 10, followed by hydrolysis and polycondensation by slowly adding water in the sol, the gel was dried at 120 °C to produce amorphous crystals, and the amorphous crystals were crushed into powders using a mortar and pestle. After the crushed powders were sieved by 120 meshes, the powders were calcinated at 700 °C using a 5 °C/min heating rate and soaked for 3 h. The nanopowders which were in order of 80–200 nm were obtained and then dispersed into NKBT sol using high-energy ball milling. Diethylene glycol abietate (BEEA) was used as dispersant. To monitor the relative effect of powder loading on electrical properties of thick films, this procedure was carried out with 0.5, 1.0, 1.5, 2.0, and 2.5 g of NKBT nanopowders for every 1 ml of precursor solution.

2.2. Screen printing and infiltration

The NKBT thick film screen-printing processing and infiltration route are shown in Fig. 1. Piezoelectric $Bi_{0.5}(Na_{0.82}K_{0.18})_{0.5}TiO_3$ powders were prepared by mixed reagent grade oxide and carbonaters at 850 °C for 4 h from TiO_2(99.5%), Bi_2O_3(98.92%), Na_2CO_3(99.8%), and K_2CO_3(99.00%). After synthesis, both powders were ball milled in acetatone for 4 h and dried. The screen-printable pastes were prepared by kneading the ground NKBT powder with 25 wt.% of organic vehicle The organic vehicle usually consists of a binder(ethyl cellulose), a solvent(α-terpineol), a plasticizer(PEG) and a dispersing agent (BEEA). The viscosity of the prepared paste was adjusted by viscosimeter in the range 20–80 Pa s for shear rate 18 s^{-1}. NKBT layers were screen-printed with a 320 mesh screen mask on 96% alumina substrates (20 mm × 15 mm × 0.5 mm), which were first electroded with an Pt paste. In order to fire the organic vehicle the layers precalcined at 550 °C for 5 min with a heating rate of 180 °C/min in rapid thermal processor (RTP).

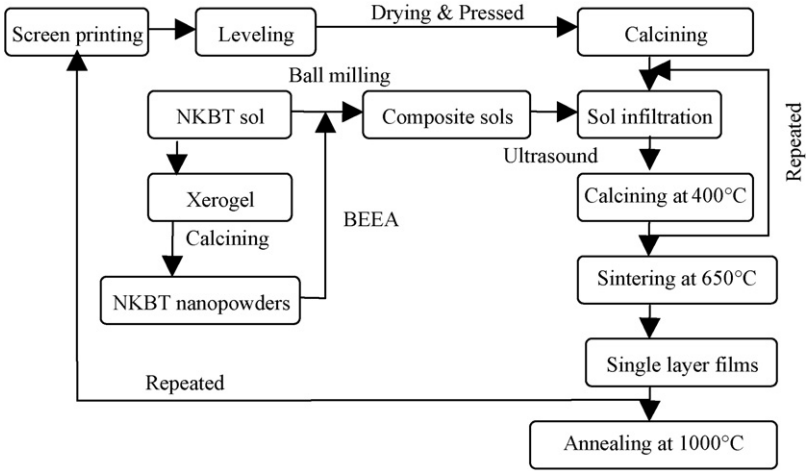

Fig. 1. NKBT thick film processing route.

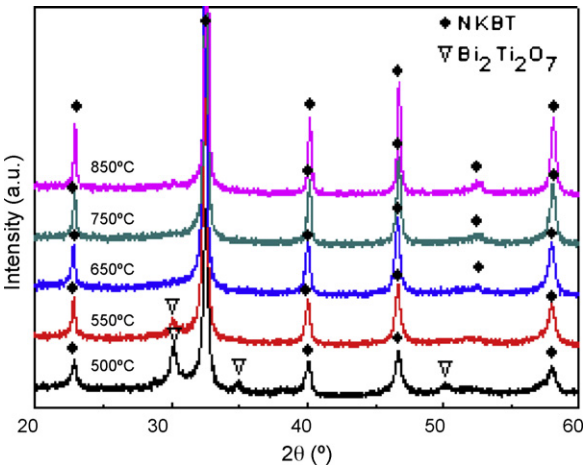

Fig. 2. X-ray powder diffraction patterns for NKBT xerogel fired at different temperatures.

The NKBT composite sols were spin coated on the precalcined NKBT thick film using a spinner operated at 2000 rpm for 30 s. These NKBT films were dried at 300 °C for 30 min to remove the organic materials. This procedure was repeated several times and once the required number of layers had been spin coated the films were subjected to a rapid thermal annealing process (650 °C/20 min) designed to crystallize them into a perovskite structure. The second layers were subsequently screen printed on the sols infiltrated thick films. After precalcination and repeated sols infiltration, the final firing of the piezoelectric thick films was performed at 1000–1100 °C for 30 min in air. These processes from printing to firing were repeated seven times to obtain about 40 μm thick lead free piezoelectric films.

2.3. Measurements

The microstructures of the thick films were examined by field-emission scanning electron microscopy (FE-SEM, Sirion 200, FEI Ltd.). Calcined powders were characterized using X-ray diffraction (X'Pert PRO, PANalytical B.V.) and the particle size was analyzed using SEM. For dielectric, ferroelectric, and piezoelectric measurements, platinum top electrodes with diameters of 0.8 mm and thickness of 0.3 μm were sputtered onto the sintered NKBT layers. The NKBT thick films were poled at 100 °C for 10 min in silicone oil. Electrical measurements were performed using an LF impedance analyzer (HP 4192A) for dielectric constant, a modified Sawyer–Tower circuit for ferroelectric hysteresis measurements, and a dual-beam laser interferometer for the longitudinal piezoelectric charge coefficient ($d_{33\text{eff}}$) measurements.

3. Results and discussion

XRD analysis was carried out to study the phase evolution of the xerogels in the calcinations process. XRD patterns of xerogels calcined at 500, 550, 650, 750, and 850 °C are shown in Fig. 2. As can be seen in the figure, $Bi_2Ti_2O_7$ cubic pyrochlore phase as reported in the JCPDS File No. 32-0118 was formed at sintering temperature lower than 650 °C.[17] When the temperature arised to 650 °C, all of the characteristic peaks of perovskite NKBT crystal appeared at 22.94, 32.58, 40.16, 46.70, 52.61, and 58.02°, and the pyrochlore phase changed to perovskite phase. After further increasing of the temperature to 750 °C and above, only diffractions belonging to perovskite NKBT were observed and there was no evidence of a second phase. The full width at half maximum of the (1 0 1) diffraction peak of NKBT powders changed from 0.217° at 650 °C to 0.167° at 850 °C. It means that the average grain size increased from 48 to 71 nm according to Scherrer's equation, indicating nanoscale dimensions of the powders.

Fig. 3 shows the dependence of the average particle size of NKBT nanopowder on aging time of precursor solution. The average particle size increases with the increasing aging time, when the NKBT precursor sol aged 36 h, cubic shape particulates of the order of 100–180 nm in size can be observed in inset picture. The increased particle size may have been due to polycondensation of the sol, in the aging procedure, the polymer cluster cross linked to form bigger cluster, the liquid phase were wrapped in the solid skeletons, and lost its mobility then turned to gel. In this procedure the differences in curvature radius of the particle clusters can result in its different solubility, which can result in different rate of growth of the cluster particles in the progress of ripening Ostward. Since the shape and size of NKBT nanopowder present strong dependence on the aging time, the precursor solution must be aged for proper time evading inhomogeneous particle size resulting short aging time and oversize particle resulting from long time aging.

Fig. 4 shows the surface and the cross-sectional SEM micrographs of the NKBT thick films with and without composite sol infiltration. The NKBT thick films without sol infiltration were of porous structure and the pore size is about 600 nm as shown in Fig. 4(a) and (b). While the films with six sol infiltrations represents crack-free interface and more smooth surface. The infiltration process results in a significant decrease of the porosity and an increase in the NKBT phase connectivity of the thick films. This is important for the improvement of the dielectric and ferroelectric properties of the thick films, because the pores

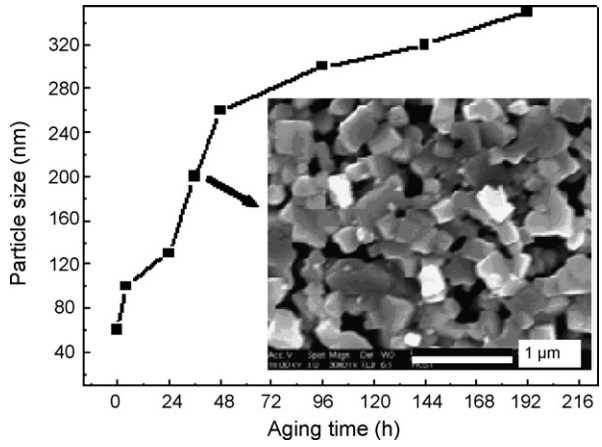

Fig. 3. The average particle size of NKBT powders with variation of aging time. Insert is SEM micrograph of NKBT powders sintered at 750 °C for 3 h (36 h aging).

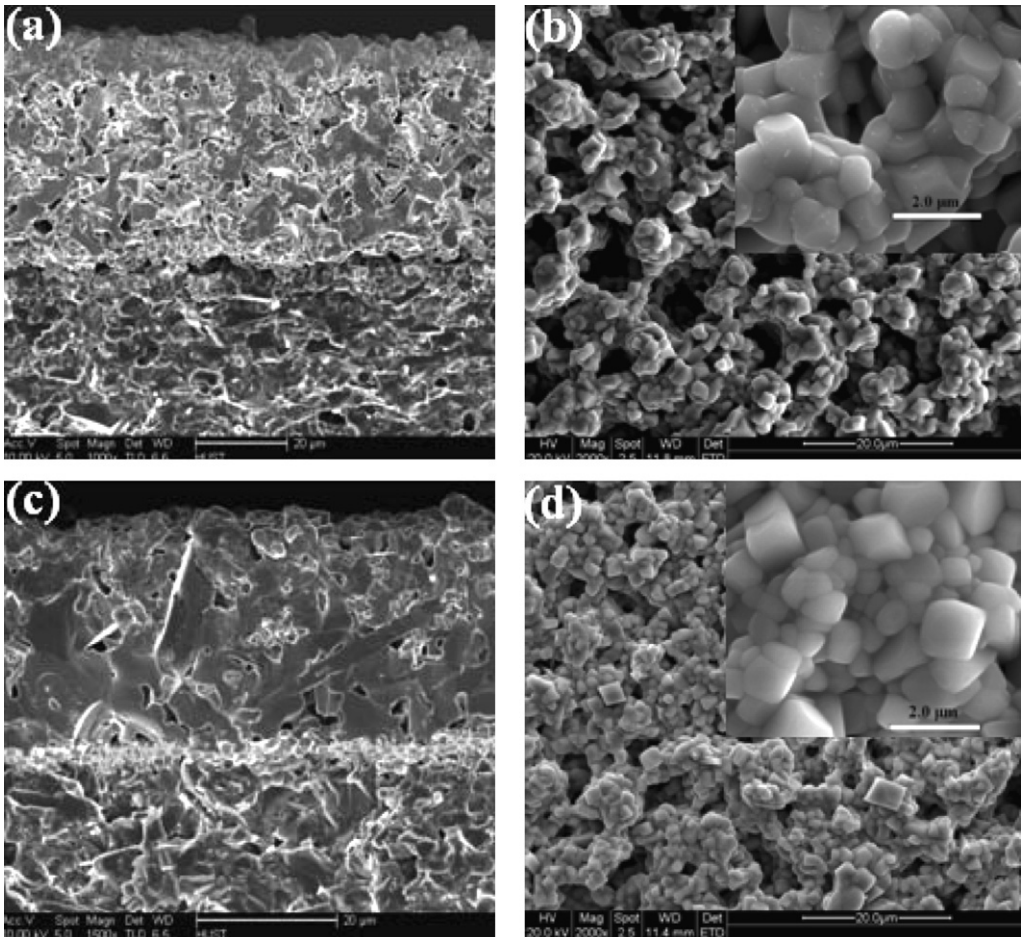

Fig. 4. SEM micrographs of the NKBT thick films: cross-sectional (a) without infiltration and (c) with 6 top infiltrations (1.5 g/ml); surface (b) without infiltration and (d) with 6 top infiltrations(1.5 g/ml).

with low dielectric constant are progressively eliminated. These results mean that the NKBT precursor composite sol which was spin coated and infiltrated between the particles and the composite sol infiltrations is a very effective method to improve the densification and homogenization of screen printed thick film structure. Moreover, the composite sol infiltration process helps to reduce the surface roughness of the thick films. As shown in Fig. 4(c), after the deposition of eight layers and six sol infiltrations, the total thickness of the NKBT thick film is about 40 μm. It is clearly seen that the composite infiltration procedure results in the drastic improvement of the microstructure, mainly in the areas close to the surface. The closed porosity in the bulk may remain in the thick films even after the six infiltrations. Compare to the pure sol infiltration by Dory et al.,[18] the composite sol infiltration can much more effectively improve the densification of the film due to its higher solid fraction.

Fig. 5 shows the relative dielectric constant, dielectric loss and relative density of NKBT thick films as a function of the powder content in composite solution. The NKBT thick films which were infiltrated by the composite precursor solution with higher solids loading (1.5 g/ml) exhibited superior dielectric properties compared with the NKBT thick film infiltrated with pure sol. The best dielectric performance of the NKBT thick films with six infiltrations were 569 and 2.8% at 10 kHz, respectively. These properties can be explained by the reduction of porosity and the increment of densification, as shown in the microstructures. When the solids loading is higher 1.5 g/ml the relative dielectric constant decreased and the dielectric loss increased with the increase in content of powder in composite solution, which may be attributed to that the NKBT thick film density cannot be improved by too high solids loading due to aggregation of the nanopowders in composite solution. As

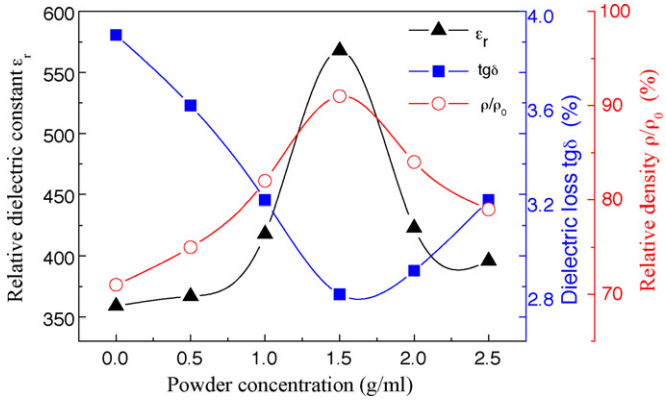

Fig. 5. Dielectric constant, dielectric loss and relative density of NKBT thick films as a function of the powder concentration of composite sols.

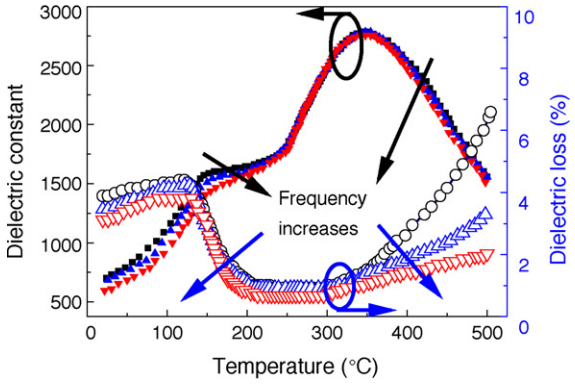

Fig. 6. Temperature dependence of the dielectric constant and dielectric loss of NKBT thick film at frequencies of 10, 100 and 1000 kHz.

shown in Fig. 5, the relative density of the NKBT thick film reaches a maximum of 91% when the film infiltrated by the composite precursor solution with 1.5 g/ml solids loading.

The dielectric constant and dielectric loss as functions of temperature for NKBT thick films infiltrated by the composite precursor solution with higher solids loading (1.5 g/ml) are shown in Fig. 6. There is a hump between room temperature and 230 °C as well as a dispersion of the dielectric constant at temperatures over 300 °C.[14] The local maximum dielectric constant and dielectric loss locate at 130 °C (T_f) and 350 °C (T_m), respectively. A phase transition from the ferroelectric to the antiferroelectric phase for NKBT thick films is observed at about 130 °C, which is consistent with a previous report.[13] The marked increase of the dielectric constant at high temperature and low frequencies is significant of space charge polarization and associated ionic conductivity. The value of dielectric constant in the local maximum decreases and its temperature is shifted upward with frequency in a way similar to that observed for typical relaxor materials. As Na^+ and Bi^{3+} are randomly distributed in the 12-fold coordination site, the relaxation behavior would reasonably attributed to some disorder induced by the presence of K^+ as well as some A-site vacancies due to the sintering process.

Fig. 7 shows the remanent polarization and coercive field of NKBT thick films. All NKBT thick films exhibited well-saturated hysteresis loops. These properties can be understood in

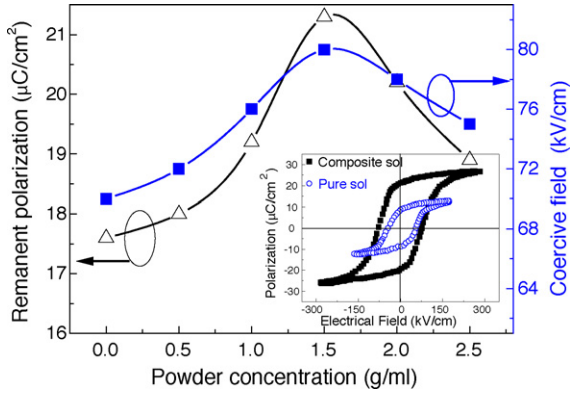

Fig. 7. Remanent polarization and coercive field of NKBT thick films as a function of the powder concentration in composite sols. Insert is *P–E* loops of NKBT thick films infiltrated with pure and composite sols.

Table 1
Electric performance of NKBT thick films with different numbers of composite sol (1.5 g/ml) infiltrations

Number of infiltrations	ε_r	$\tan\delta$ (%)	P_r (μC/cm²)	E_c (kV/cm)	d_{33eff} (pm/V)
0	427	4.6	10.4	46	56
3	531	3.4	17.5	63	81
6	569	2.8	21.3	80	109
9	579	2.8	21.8	83	110
12	585	2.7	22.6	82	112

terms of the effects of densification and reduction of poresize.[19] The porosity which created the depolarizing field decreased with the increase in the number of sol coatings. A remanent polarization P_r of 21.3 μC/cm² and a coercive field E_c of 80 kV/cm were obtained for the NKBT thick film by composite sol infiltration. The remanent polarization of the thick film was smaller than that of the bulk NBT–KBT–BT ceramics (P_r = 35.9 μC/cm²).[20] This is due to the pores remaining in the thick films. The coercive field of the thick film was higher than that of the bulk ceramics. Maybe this is due to the clamping effects of the films by the substrate. Ferroelectric hysteresis loops shown in Fig. 7 insert indicate that the NKBT thick films derived from composite sol infiltration exhibit higher remanent polarization and coercive field than that derived form pure sol infiltration. The increase of the coercive field attribute to increasing breakdown field resulting from the decrease of the surface roughness and bulk porosity.

As shown in Table 1 dielectric constant, remanent polarization, and coercive field increase with increasing number of top infiltration layers. As already mentioned, these values were obtained due to the progressive elimination of porosity. The decrease of the surface roughness is also essential, since it allows application of high voltage without significant leakage. Therefore, the shape of the loop does not show any sign of leakage contribution. As the pore size is progressively reduced with infiltration, the infiltration becomes more difficult. This results in the saturation of the relative permittivity and remanent polarization values.

The composite sol derived films in pores of the thick films can be modeled as 0–3 composite material,[21] where the sol–gel matrix is fully connected in three directions and the NKBT nanopowders are not connected in any direction. If the nanopowders are uniformly dispersed in the sol–gel matrix then the resulting dielectric constant is given by

$$\varepsilon_m = \varepsilon_s \left(1 + \frac{3V_p(\varepsilon_p - \varepsilon_s)}{\varepsilon_p + 2\varepsilon_s - V_p(\varepsilon_p - \varepsilon_s)}\right) \quad (1)$$

where ε_s is the dielectric constant of the sol–gel matrix, ε_p is the dielectric constant of NKBT nanopowder, and V_p is the volume fraction of the nanopowder. In practice, the above equation is only valid for values of V_p <10%, because at higher concentrations, the dispersed phase starts to form continuous structures throughout the bulk. It then becomes necessary to treat the composite as having phases connected in both series and parallel, and the dielectric constant is given by

$$\varepsilon_{cp} = V_p\varepsilon_p + V_s\varepsilon_s \quad (2)$$

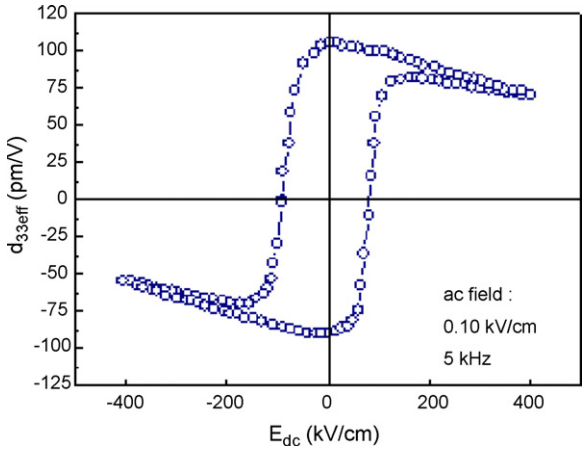

Fig. 8. Piezoelectric charge coefficient d_{33} as a function of dc electric field of the NKBT thick films with 6 top infiltrations (1.5 g/ml).

$$\varepsilon_{cs} = \left(\frac{V_s}{\varepsilon_s} + \frac{V_p}{\varepsilon_p}\right)^{-1} \quad (3)$$

where V_s is the volume fraction of sol–gel matrix, the composite sol film exists in a combination of series and parallel phases, and the dielectric constant is then:

$$\varepsilon_c = \varepsilon_s(1 - V_p^{2/3}) + \frac{\varepsilon_s\varepsilon_p}{(\varepsilon_s - \varepsilon_p)V_p^{-1/3} + \varepsilon_p V_p^{-2/3}} \quad (4)$$

We shall assume that the pores, infiltrated by composite sols, are uniformly dispersed in thick film matrix. When the volume fraction of the pores, $V_{pore} < 10\%$, the dielectric constant of the composite infiltrated NKBT thick films is given by

$$\varepsilon = \varepsilon_{pr}\left(1 + \frac{3V_{pore}(\varepsilon_c - \varepsilon_{pr})}{\varepsilon_c + 2\varepsilon_{pr} - V_{pore}(\varepsilon_c - \varepsilon_{pr})}\right) \quad (5)$$

where V_{pore} is the volume fraction of the pores, and ε_{pr} is the dielectric constant of the thick films without sol infiltration, and ε_c is the dielectric constant of composite sol films in pores.

The effective longitudinal d_{33eff} piezoelectric coefficient as a function of dc electric field is shown in Fig. 8. The piezoelectric coefficient d_{33eff} demonstrates a clear switching behavior. The value of remanent d_{33eff} of the NKBT thick film with six composite sol infiltration layers reaches high values of 100–110 pm/V when the positive bias is applied to the top electrode. The value is the highest reported in the literature, however, is still lower than the bulk values due to clamping effect of the substrate, residual porosity and small grain size. This value is comparable to that in PZT thick films produced by screen printing.[22] The measured effective parameter d_{33eff} and the effect of clamping to the substrate is as following function:

$$d_{33eff} = \frac{S_3}{E_3} = d_{33} - \frac{2d_{31}S_{13}^E}{S_{11}^E + S_{12}^E} \quad (6)$$

where S_{13}^E, S_{11}^E, and S_{12}^E are the elastic compliance, and d_{33}, d_{31} are the free longitudinal, transversal piezoelectric coefficient respectively. Since $d_{31} < 0$, $S_{13}^E < 0$, $S_{11}^E + S_{12}^E < 0$, the measured effective d_{33eff} is always smaller than in free materials. As follows from Torah et al. there is approximately 74% reduction in the measured d_{33eff} value.[23] The d_{33eff} asymmetry, difference between positive and negative poling, can be explained by the difference between the two interfaces and inhomogeneous electric field distribution under poling. As a result, higher piezoelectric properties are observed under positive poling.

4. Conclusion

It is shown that the dielectric, ferroelectric and piezoelectric properties of the screen printing NKBT thick films can be significantly improved by using infiltration with corresponding composite sols. The composite sols containing precursor solution and nanopowders with same composition are used to replace the pure sols in thick film infiltration treatment. The porosity is significantly reduced along with the roughness of the surface. Crack-free dense NKBT thick films deposited on Pt electroded alumina substrates show remanent polarization, dielectric constant and dielectric loss almost identical to the bulk ceramics values. The best dielectric performance of the NKBT thick films with six infiltrations were 569 and 2.8% at 10 kHz, respectively. The value of remanent d_{33eff} of the film with six composite sol infiltration layers reaches high values of 100–110 pm/V when the positive bias is applied to the top electrode. The piezoelectric coefficient is lower due to the clamping effect of the substrate and small grain size. The thick films is expected to be a new and promising candidate for lead-free piezoelectric MEMS especially the micro actuators applications.

Acknowledgements

This research was partially supported by National High Technology Research and Development Program of China (No. 2007AA03Z120), the National Natural Science Foundation of China (No. 60777043), and Program for New Century Excellent Talents in University (NCET-04-0703). The authors also wish to thank the Analytical and Testing Center of Huazhong University of Science and Technology for XRD and SEM analysis.

References

1. Koch, M., Harris, N., Evans, A. G. R., White, N. M. and Brunnschweiler, A., A novel micromachined pump based on thick-film piezoelectric actuation. *Sens. Actuators A*, 1998, **70**, 98–103.
2. Kim, Y.-B., Kim, H.-J., Cheon, C. I., Choi, D.-J. and Kim, T. S., Preparation of diffuser type micropump using screen-printed PZT–PCW thick films. *Integr. Ferroelectr.*, 2002, **50**, 61–70.
3. Morita, T., Kurosawa, M. and Higuchi, T., Design of a cylindrical ultrasonic micromotor to obtain mechanical output. *Jpn. J. Appl. Phys.*, 1996, **35**, 3251–3254.
4. Yan, T., Jones, B. E., Rakowski, R. T., Tudor, M. J., Beeby, S. P. and White, N. M., Design and fabrication of thick-film PZT-metallic triple beam resonators. *Sens. Actuators A*, 2004, **115**, 401–407.
5. Harris, N. R., Hill, M., White, N. M. and Beeby, S. P., Acoustic power output measurements for thick-film PZT transducers. *Electron. Lett.*, 2004, **40**, 636–637.
6. Marechal, P., Levassort, F., Holc, J., Tran-Huu-Hue, L.-P., Kosec, M. and Lethiecq, M., High-frequency transducers based on integrated piezoelectric thick films for medical imaging. *IEEE Trans. Ultrason. Ferroelectr. Freq. Control*, 2006, **53**, 1524–1533.

7. Wang, S., Lam, K. H., Sun, C. L., Kwok, K. W., Chan, H. L. W., Guo, M. S. *et al.*, Energy harvesting with piezoelectric drum transducer. *Appl. Phys. Lett.*, 2007, **90**, 113506.
8. Saito, Y., Takao, H., Tani, T., Nonoyama, T., Takatori, K., Homma, T. *et al.*, Lead-free piezoceramics. *Nature*, 2004, **432**, 84–87.
9. Yu, T., Kwok, K. W. and Chan, H. L. W., The synthesis of lead-free ferroelectric $Bi_{0.5}Na_{0.5}TiO_3$-$Bi_{0.5}K_{0.5}TiO_3$ thin films by sol–gel method. *Mater. Lett.*, 2007, **61**, 2117–2120.
10. Nagata, H. and Takenaka, T., Lead-free piezoelectric ceramics of $(Bi_{1/2}Na_{1/2})TiO_3$–$(1/2)(Bi_2O_3{\cdot}Sc_2O_3)$ system. *Jpn. J. Appl. Phys.*, 1997, **36**, 6055–6057 [Publication Office, Kyoto, Japan].
11. Nagata, H., Shinya, T., Hiruma, Y., Takenaka, T., Sakaguchi, I. and Haneda, H., Piezoelectric properties of bismuth sodium titanate ceramics. In American Ceramic Society, Westerville, OH 43086-6136/Indianapolis, IN, United States, 2005, vol. **167**, pp. 213–221.
12. Nagata, H., Yoshida, M., Makiuchi, Y. and Takenaka, T., Large piezoelectric constant and high curie temperature of lead-free piezoelectric ceramic ternary system based on bismuth sodium titanate-bismuth potassium titanate-barium titanate near the morphotropic phase boundary. *Jpn. J. Appl. Phys.*, 2003, **42**, 7401–7403.
13. Isupov, V. A., Ferroelectric $Na_{0.5}Bi_{0.5}TiO_3$ and $K_{0.5}Bi_{0.5}TiO_3$ perovskites and their solid solutions. *Ferroelectrics*, 2005, **315**, 123–147.
14. Sasaki, A., Chiba, T., Mamiya, Y. and Otsuki, E., Dielectric and piezoelectric properties of $(Bi_{0.5}Na_{0.5})TiO_3$–$(Bi_{0.5}K_{0.5})TiO_3$ systems. *Jpn. J. Appl. Phys.*, 1999, **38**, 5564–5567.
15. Yao, K., He, X., Xu, Y. and Chen, M., Screen-printed piezoelectric ceramic thick films with sintering additives introduced through a liquid-phase approach. *Sens. Actuators A*, 2005, **118**, 342–348.
16. Lee, S.-G., Effects of sol infiltration on the screen-printed lead zirconate titanate thick films. *Mater. Lett.*, 2007, **61**, 1982–1985.
17. Hector, A. L. and Wiggin, S. B., Synthesis and structural study of stoichiometric $Bi_2Ti_2O_7$ pyrochlore. *J. Solid State Chem.*, 2004, **177**, 139–145.
18. Dorey, R. A., Stringfellow, S. B. and Whatmore, R. W., Effect of sintering aid and repeated sol infiltrations on the dielectric and piezoelectric properties of a PZT composite thick film. *J. Eur. Ceram. Soc.*, 2002, **22**, 2921–2926.
19. Okazaki, K. and Nagata, K., Effects of grain size and porosity on electrical and optical properties of plzt ceramics. *J. Am. Ceram. Soc.*, 1973, **56**, 82–86.
20. Wang, X. X., Tang, X. G. and Chan, H. L. W., Electromechanical and ferroelectric properties of $(Bi_{1/2}Na_{1/2})TiO_3$–$(Bi_{1/2}K_{1/2})TiO_3$-$BaTiO_3$ lead-free piezoelectric ceramics. *Appl. Phys. Lett.*, 2004, **85**, 91–93.
21. Newnham, R. E., Skinner, D. P. and Cross, L. E., Connectivity and piezoelectric-pyroelectric composites. *Mater. Res. Bull.*, 1978, **13**, 525–536.
22. Thiele, E. S., Damjanovic, D. and Setter, N., Processing and properties of screen-printed lead zirconate titanate Piezoelectric thick films on electroded silicon. *J. Am. Ceram. Soc.*, 2001, **84**, 2863–2868.
23. Torah, R. N., Beeby, S. P. and White, N. M., Experimental investigation into the effect of substrate clamping on the piezoelectric behaviour of thick-film PZT elements. *J. Phys. D: Appl. Phys.*, 2004, **37**, 1074–1078.